Chinese Chemical Letters 35 (2024) 109516

Contents lists available at ScienceDirect

Chinese Chemical Letters

journal homepage: www.elsevier.com/locate/cclet

Curing the vulnerable heterointerface *via* organic-inorganic hybrid hole transporting bilayers for efficient inverted perovskite solar cells

Kangrong Yan[1], Ziqiu Shen[1], Yanchun Huang[1], Benfang Niu, Hongzheng Chen, Chang-Zhi Li*

State Key Laboratory of Silicon and Advanced Semiconductor Materials, Department of Polymer Science and Engineering, Zhejiang University, Hangzhou 310027, China

ARTICLE INFO

Article history:
Received 27 October 2023
Revised 4 January 2024
Accepted 5 January 2024
Available online 12 January 2024

Keywords:
Perovskite solar cells
Conjugated polymer
Hole transporting bilayer
Charge extraction
Heterointerface degradation

ABSTRACT

To promote the practices of perovskite photovoltaics, it requires to develop efficient perovskite solar cells (PVSCs) standing long-time operation under the adverse environments. Herein, we demonstrate that the tailor-made conjugated polymers as conductive adhesives stabilized the originally redox-reactive heterointerface between perovskite and metal oxide, facilitating the access of efficient and stable inverted PVSCs. It was revealed that bithiophene and phenyl alternating conjugated polymers with partial glycol chains atop of the metal oxide layer has resulted in effective organic-inorganic hybrid hole transporting bilayers, which allow maintaining efficient hole extraction and transport, meanwhile preventing halide migration to directly contact with the nickel oxide (NiO_x) layer. As a result, the corresponding inverted PVSCs with the organic-inorganic hole transporting bilayers have achieved an excellent power conversion efficiency of 23.22%, outperforming 20.65% of bare NiO_x-based devices. Moreover, the encapsulated PVSCs with organic-inorganic bilayers exhibited the excellent photostability with 91% of the initial efficiency after 1000-h one-sun equivalent illumination in ambient conditions. Overall, this work provides new insights into stabilizing the vulnerable heterointerface for perovskite solar cells.

Solar photon-to-electron conversion *via* photovoltaics allows powering the sustainable communities with desirable environmental friendliness. In recent years, the emerging lead halide perovskites exhibit great promises to be deployed as solution-processed, high-efficiency photovoltaics [1–3]. The state-of-the-art perovskite solar cells (PVSCs) have reached high power conversion efficiencies (PCEs) of over 26% [4]. Though encouraging progresses have been made, concerns remain to question whether the operational stabilities of PVSCs can stand under long-term illumination [5–7]. Indeed, three-dimensional lead halide perovskites are prone to degradation when encountering the irreversible chemical reaction of components, *i.e.*, ammonium decomposition and halide oxidation [6,8]. For instance, wide-bandgap metal oxides, such as nickel oxide (NiO_x), widely employed as the hole transporting layer (HTL) in inverted PVSCs [9–14], have contained not only abundant surface defects to constrain charge extraction [15], but also possessed the photoinduced reactivities, *i.e.*, the redox reaction with halides [16–18], to degrade perovskites [19]. Interfacial strategies, including element doping [20], self-assembled monolayer [21], and hybrid bilayer [22], have been developed to primarily optimize charge extraction of the metal oxide HTLs. However, the undesirable chemical reaction at the HTL/perovskite heterointerface has destructed operational stabilities of bare NiO_x-based PVSCs, yet requiring further studies [18]. Toward practical relevance, high efficiencies and long lifetimes need to be simultaneously embedded in perovskite photovoltaics.

Herein, we developed a strategy of organic-inorganic hybrid charge extraction bilayers, which helped not only boosting interfacial charge extraction, but more importantly stabilizing the heterointerfaces from chemical degradation, to facilitate the access of efficient and stable inverted PVSCs. It reveals that the introduction of tailor-made conjugated polymers with partial glycol chains atop of the metal oxide layer has resulted in effective organic-inorganic hybrid bilayers, which allow maintaining efficient hole extraction and transport, meanwhile preventing halide migration to react with the NiO_x layer. It therefore resolved the issues of redox reaction between perovskite and the NiO_x hole selective layer, meanwhile providing a suitable underlayer to promote the growth of crystalline perovskite films. As results, the corresponding device exhibited excellent photovoltaic performances with the best

* Corresponding author.
E-mail address: czli@zju.edu.cn (C.-Z. Li).
[1] These authors contributed equally to this work.

https://doi.org/10.1016/j.cclet.2024.109516
1001-8417/

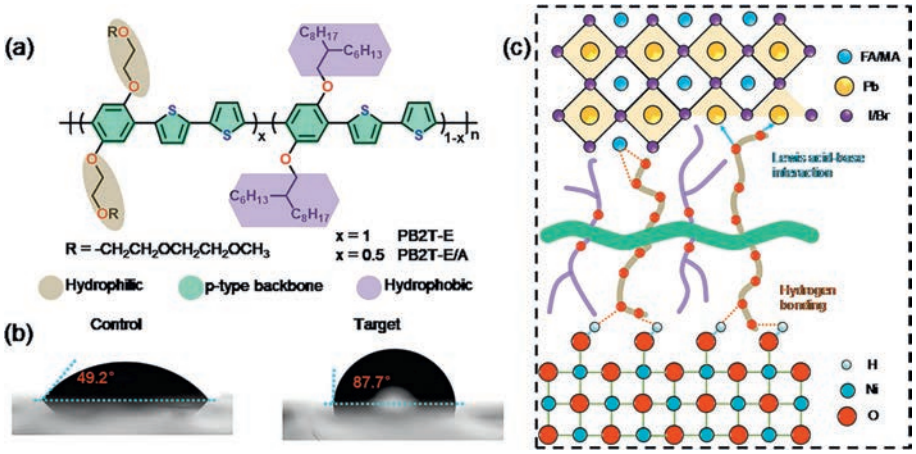

Fig. 1. Design of functional conjugated polymers. (a) Chemical structures of conjugated polymers. (b) Water contact angles on the control, P-E-N and target HTL substrates. (c) Schematic illustration of interactions among polymer with NiO_x and perovskite.

PCE of 23.22% in inverted PVSCs, outperforming those based on bare NiO_x layer (the best PCE of 20.65%). In addition, the organic-inorganic hybrid bilayers have elongated the lifetime of the encapsulated PVSCs, maintaining 91% of the initial efficiency after 1000-h one-sun equivalent illumination in ambient conditions. Overall, this work provides an effective strategy to cure the vulnerable heterointerface, hence enhancing the photovoltaic performance and operational stability of inverted perovskite solar cells.

Note that the solution fabrication of perovskite films has mostly accomplished atop of charge transporting layers (CTLs) in planar PVSCs [23–26], wherein the heterointerface properties between CTL and perovskite critically impact on the performance and stabilities of PVSCs [27,28]. In inverted PVSCs, it was identified that high-valence $Ni^{\geq 3+}$ sites of NiO_x show the redox reactivity with halides of perovskites. In this work, p-type functional conjugated polymers, PB2T-E and PB2T-E/A (Fig. 1a) consisting of alternative bithiophene and phenyl group with the varied sidechains, are developed *via* Stille coupling [25,29–31]. The synthetic and characterization details can be found in Supporting information (Schemes S1 and S2, Figs. S1–S6). Fig. S7 (Supporting information) showed the absorption and photoluminescence (PL) spectra of the two polymers, resulting in similar optical properties. The lowest unoccupied molecular orbital (LUMO) and highest occupied molecular orbital (HOMO) levels, obtained from cyclic voltammograms (Fig. S7c), are −3.56 eV and −5.00 eV for PB2T-E, −3.52 eV and −5.06 eV for PB2T-E/A, respectively. These polymers possess excellent thermal stabilities and hole transporting capabilities, with hole mobilities of 1.89×10^{-4} and 1.58×10^{-4} cm^2 s V^{-1} for PB2T-E and PB2T-E/A, respectively (Fig. S8 in Supporting information). Note the varied hydrophilic methoxy triglycol and hydrophobic 2-hexyldecayl sidechains are employed to adjust the solubility and surface wettability of polymers, changing the water contact angles from 49.2° (NiO_x) to 55.3° and 87.7° for PB2T-E and PB2T-E/A atop of NiO_x, respectively (Fig. 1b and Fig. S9 in Supporting information). PB2T-E with solely glycol chains shows certain solubilities in polar *N,N'*-dimethyl formamide (DMF) and dimethyl sulfoxide (DMSO) solvents, which could be partially washed out during subsequent fabrication of the perovskite precursor solution. Encouragingly, PB2T-E/A with half hydrophilic glycol chains and half hydrophobic alkyl chains exhibits excellent orthogonal-solvent processability and tolerance towards post-fabrication. Therefore, we referred to hereafter bare NiO_x as control and PB2T-E/A atop of NiO_x bilayers as target for comparison studies, and we envision that such functional polymers could serve as conductive adhesives to modulate the heterointerface properties between HTL and perovskite (Fig. 1c).

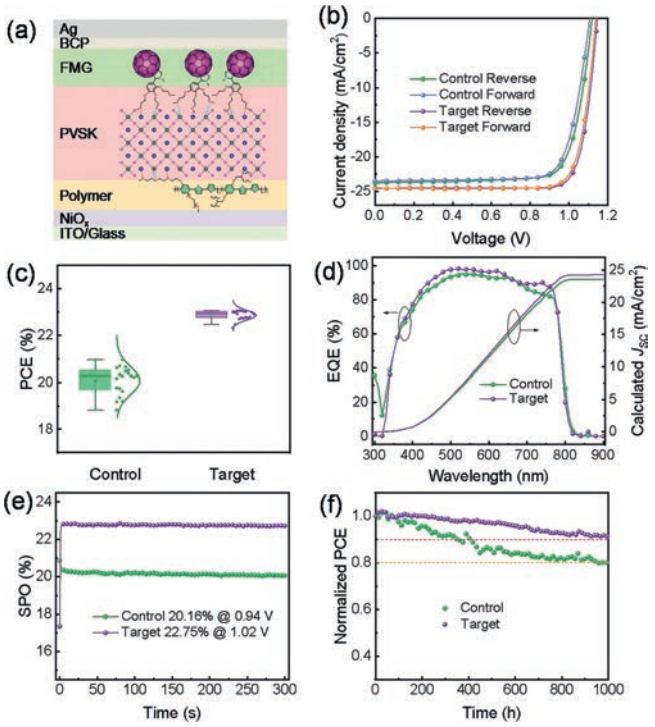

Fig. 2. Photovoltaic performances of different PVSCs. (a) The schematic architecture of the studied PVSCs. (b) *J-V* curves at reverse and forward scanning, (c) PCE histograms, (d) EQE spectra and (e) steady power outputs of PVSCs with control and target HTLs. (f) Normalized PCE of encapsulated PVSCs on the control and target HTLs under continuous one sun-equivalent illumination in ambient conditions.

To exam their photovoltaic properties, we first fabricated inverted PVSCs with the architecture of ITO/HTL/perovskite/FMG/BCP/Ag (Fig. 2a), wherein FMG is a fullerene-based electron transporting material with glycol sidechains [32], and the HTL refers to bare NiO_x (control) and NiO_x/PB2T-E/A bilayer (target), respectively. The current density-voltage (*J-V*) curves at reverse and forward scanning under 100 mW/cm^2 of simulated AM 1.5 G illumination are shown in Fig. 2b. The corresponding photovoltaic parameters are summarized in Table S1 (Supporting information). PCEs of 20.65% and 23.22% are obtained for inverted PVSCs based on the control and target HTLs (Table S2 in Supporting information). It suggests the incorporation of conjugated polymers plays roles to modulate the NiO_x/perovskite heterointerface to improve

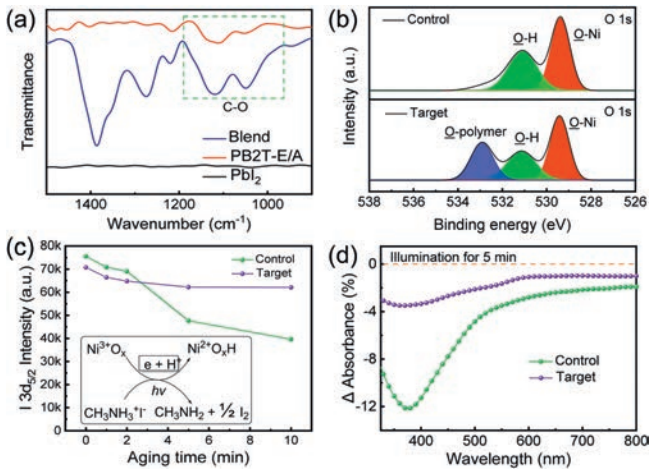

Fig. 3. Molecular interaction and perovskite degradation. (a) FTIR spectroscopy of PbI_2, PB2T-E/A and their blend. (b) XPS spectra of O 1s for control and target HTLs. (c) The intensity of I $3d_{5/2}$ signals along with different aging time; insert figure: proposal degradation pathway of MAI on pristine NiO_x films. (d) UV–vis absorbance difference of MAI atop of different HTLs before and after 5 min UV illumination.

the photovoltaic performance of PVSCs. The target devices obtained simultaneously improvements on the open-circuit voltage (V_{OC}), short-circuit current density (J_{SC}) and fill factor (FF) over those of control devices. And the devices based on NiO_x/PB2T-E bilayers also obtained the increased device parameters (PCE of 22.13%, Fig. S10 in Supporting information), compared to control devices. It is interesting to note that, comparing to the PB2T-E with solely hydrophilic glycol sidechains, PB2T-E/A with mixed hydrophilic and hydrophobic sidechains promoted the derived PVSCs with improved charge extraction and reduced charge recombination, along with the excellent reproducibility of narrow distribution of efficiency histograms (Fig. 2c). The trap state densities of the corresponding devices, 5.52×10^{15} cm^{-3} (control) and 2.27×10^{15} cm^{-3} (target), were estimated from space charge limited current (SCLC) experiments with the trap-filled limit voltages (V_{TFL}) of 0.39 and 0.16 V, respectively (Fig. S11 in Supporting information).

The calculated J_{SC} from the integral values of external quantum efficiency (EQE) spectra match well with experimental values (Fig. 2d). The steady power outputs (SPO) are stable as a function to time at the maximum voltage (Fig. 2e). The operational stabilities at the maximum power points (MPP) of the encapsulated PVSCs with control and target HTLs have been compared under continuous one-sun equivalent illumination in ambient conditions. The target PVSC showed excellent operational stability and remain 91% of the initial PCE after continuous 1000-h illumination, better than the control device with maintaining 80% of its initial value (Fig. 2f). These results revealed that the introduction of tailor-made polymers atop of NiO_x layer has resulted in effective organic-inorganic hybrid hole transporting bilayers, which could not only improve the photovoltaic performance, but also elongate the operational lifetime of the corresponding PVSCs. We ascribe that the newly designed polymers provide desirable molecular interaction to modify the heterointerface between perovskite and NiO_x layers, which allows maintaining efficient hole extraction and transport, meanwhile avoiding halide reaction with NiO_x layer.

To understand molecular interactions of polymers with NiO_x and perovskites, we employed Fourier-transform infrared (FTIR) spectroscopy [33,34] to analyze the characteristic peaks of polymer and polymer-inorganic composites (Fig. 3a and Fig. S12 in Supporting information). There presents Lewis acid-base interaction between PB2T-E/A and PbI_2 (Fig. 3a), revealed from the increased intensities of C–O peaks over that of the neat polymer. It is also known that glycol chains of polymers possessed hydrogen bonding interactions to the ammonium of perovskites [32,35]. Similar results were observed from FTIR measurements of PB2T-E and its blends (Fig. S12). The proper molecular interaction between perovskites and organic materials allows passivating the grain defects of perovskites [36–39]. These results suggest that new functional polymers not only interact with ammonium moieties *via* hydrogen bonding, but also coordinate with lead ions in perovskites.

X-ray photoelectron spectroscopy (XPS) reveals the coating of PB2T-E/A onto the NiO_x film subtly altered the chemical states of O elements in NiO_x, which would be ascribed to the possible passivation of NiO_x with the polymer coating (Fig. 3b and Fig. S13 in Supporting information). Interestingly, the change of XPS patterns was monitored for model samples consisting of methylammonium iodide (MAI) atop of control and target HTLs, respectively (Fig. S14 in Supporting information). The large decrease of I $3d_{5/2}$ intensities was observed for MAI atop of control films along with different aging time of UV-illumination, indicating the redox reaction between iodide of MAI and NiO_x (Fig. 3c). In the large contrast, there showed little change of I $3d_{5/2}$ intensities for MAI atop of target films upon UV-illumination, suggesting PB2T-E/A can help suppressing the photo degradation at the perovskite/HTL heterointerface. It is because the insert of a dense conjugated polymer layer could physically isolate and prevent halide migration to directly contact with NiO_x, therefore avoiding the heterointerface degradation. Meanwhile, conjugated polymers with high charge mobilities also maintained the efficient hole extraction and transport. Similarly, absorption spectra were carried out to record the absorption difference of MAI/NiO_x films before and after UV-illumination, revealing the redox reaction between NiO_x and MAI with the generation of strong iodine absorption peaks (Fig. 3d). Whereas the sample with MAI atop of the target HTL appeared little change of absorption spectra before and after illumination, affirming that PB2T-E/A can help stabilizing perovskite/HTL heterointerface.

In addition to molecular interaction, the modulation of bottom surfaces can make large impacts on the film formation of perovskites fabricated atop [23]. Scanning electron microscopy (SEM) measurements were conducted to characterize the morphologies of perovskite films on different HTLs (Fig. 4). From top-view SEM images (Figs. 4a and b), it shows that the average grain sizes of perovskite atop of the hydrophobic bilayer HTL (target) are generally larger than that atop of hydrophilic NiO_x HTL (control). The grain size distributions for perovskites on various HTLs are summarized in Fig. S15 (Supporting information), and the average sizes of perovskite grains are 440 nm and 500 nm on control and target HTLs, respectively. Similarly, there also appears clear distinction for vertical morphologies of perovskites films atop of the varied HTLs from cross-sectional SEM images (Figs. 4c and d). Perovskites atop of the bilayer HTLs (target) exhibit vertical-orientated and continuous grains. While mainly small and discontinuous grains are observed for perovskites grown atop of bare NiO_x. X-ray diffraction (XRD) patterns for perovskites atop of different HTLs were conducted (Fig. 4e) to reveal that the peaks at 14.01° (100) and 24.35° (111) of perovskite on the target HTL had stronger intensities than that of the control HTL, consistent with the SEM results, suggesting that the target HTL could facilitate the crystal growth of perovskite films.

Steady-state PL reveals the efficient PL quenching was observed for perovskite atop of the target HTL (Fig. S16 in Supporting information), demonstrating effective charge extraction from perovskite to the target HTL. Moreover, time-resolved photoluminescence (TRPL) measurements (Fig. 4f and Table S3 in Supporting information) suggested the fast hole extraction from perovskite to the target HTL with the average decay time (τ) of 2.06 ns, which was much faster than that of the control HTL ($\tau = 15.61$ ns). This information above clearly revealed that good quality perovskite

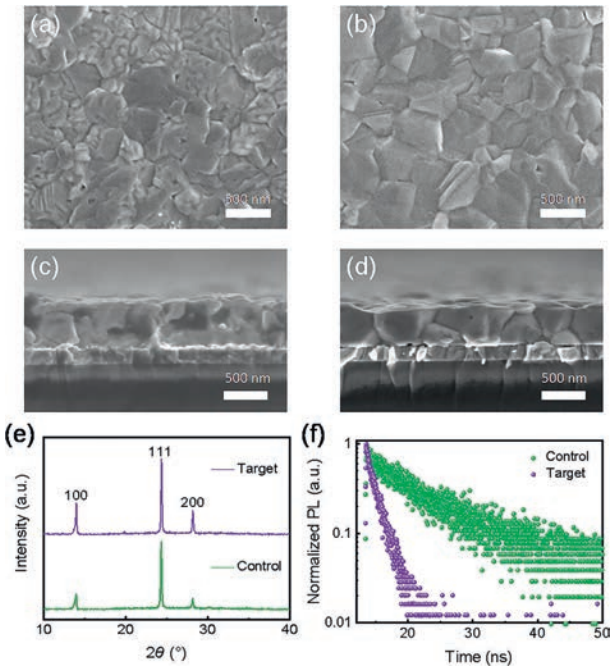

Fig. 4. Morphologies and charge dynamics of perovskite films on varied HTLs. (a, b) Top-view and (c, d) cross-sectional SEM images of perovskite films on the control and target HTLs. (e) XRD patterns of the perovskite films on different HTLs. (f) TRPL spectra of perovskite films fabricated at different HTLs.

films, together with efficient and stable hole extraction, can be obtained from the introduction of bilayer HTLs to perovskites.

In summary, new functional polymers are developed as conductive adhesives to effectively cure the unstable heterointerface between metal oxide and perovskite, meanwhile maintaining the efficient hole extraction and transport, which facilitated the access of efficient and stable inverted PVSCs. As a result, inverted PVSCs with the introduction of organic-inorganic hybrid hole transporting bilayers not only obtained an excellent PCE of 23.22%, higher than that of control PVSCs with bare NiO_x (20.65%). Moreover, such hybrid bilayer HTLs also endowed the excellent photostability of the encapsulated PVSCs, maintaining over 90% of the initial efficiency after 1000-h illumination aging in ambient conditions. Overall, this work provides an effective strategy to stabilize the vulnerable heterointerface for efficient and stable inverted perovskite solar cells.

Declaration of competing interest

The authors declare that they have no known competing financial interests or personal relationships that could have appeared to influence the work reported in this paper.

Acknowledgments

This research was funded by the National Natural Science Foundation of China (No. 22125901), the National Key Research and Development Program of China (No. 2019YFA0705900), the Fundamental Research Funds for the Central Universities (No. 226–2023–00113).

Supplementary materials

Supplementary material associated with this article can be found, in the online version, at doi:10.1016/j.cclet.2024.109516.

References

[1] X. Luo, X. Lin, F. Gao, et al., Sci. China Chem. 65 (2022) 2369–2416.
[2] H. Zhu, S. Teale, M.N. Lintangpradipto, et al., Nat. Rev. Mater. 8 (2023) 569–586.
[3] Q. Tan, Z. Li, G. Luo, et al., Nature 620 (2023) 545–551.
[4] M.A. Green, E.D. Dunlop, M. Yoshita, et al., Prog. Photovolt. Res. Appl. 31 (2023) 651–663.
[5] D. Yu, Y. Hu, J. Shi, et al., Sci. China Chem. 62 (2019) 684–707.
[6] C.C. Boyd, R. Cheacharoen, T. Leijtens, et al., Chem. Rev. 119 (2019) 3418–3451.
[7] W. Fu, A.G. Ricciardulli, Q.A. Akkerman, et al., Mater. Today 58 (2022) 275–296.
[8] D. Zhang, D. Li, Y. Hu, et al., Commun. Mater. 3 (2022) 58.
[9] P. Qin, Q. He, D. Ouyang, et al., Sci. China Chem. 60 (2017) 472–489.
[10] L. Xu, X. Chen, J. Jin, et al., Nano Energy 63 (2019) 103860.
[11] F. Ma, Y. Zhao, J. Li, et al., J. Energy Chem. 52 (2021) 393–411.
[12] H. Zhang, C. Zhao, J. Yao, et al., Angew. Chem. Int. Ed. 62 (2023) e202219307.
[13] Y. Yu, P. Gao, Chin. Chem. Lett. 28 (2017) 1144–1152.
[14] Y. Yang, N.D. Pham, D. Yao, et al., Chin. Chem. Lett. 29 (2018) 1242–1250.
[15] F. Wu, K. Yan, H. Wu, et al., Chin. J. Chem. 40 (2022) 2694–2700.
[16] A. Singh, S.L.Y. Chang, R.K. Hocking, et al., Energy Environ. Sci. 6 (2013) 579–586.
[17] M. Bonomo, D. Dini, A.G. Marran, Langmuir 32 (2016) 11540–11550.
[18] C.C. Boyd, R.C. Shallcross, T. Moot, et al., Joule 4 (2020) 1759–1775.
[19] S. Ahmad, R. Ma, J. Zheng, et al., Small Methods 6 (2022) e2200787.
[20] W. Chen, Y. Wu, Y. Yue, et al., Science 350 (2015) 944–948.
[21] H. Liu, K. Yan, J. Rao, et al., ACS Appl. Mater. Interfaces 14 (2022) 6794–6800.
[22] B. Niu, H. Liu, Y. Huang, et al., Adv. Mater. 35 (2023) 2212258.
[23] C. Bi, Q. Wang, Y. Shao, et al., Nat. Commun. 6 (2015) 7747.
[24] C. Huang, W. Fu, C.Z. Li, et al., J. Am. Chem. Soc. 138 (2016) 2528–2531.
[25] Z. Zhang, W. Fu, H. Ding, et al., Adv. Mater. Interfaces 5 (2018) 1800090.
[26] F. Ullah, H.Z. Chen, C.Z. Li, Chin. Chem. Lett. 28 (2017) 503–511.
[27] T. Wang, W. Deng, J. Cao, et al., Adv. Energy Mater. 13 (2022) 2201436.
[28] N. Chen, D. Luo, P. Chen, et al., ACS Energy Lett. 8 (2023) 1313–1321.
[29] C.G. Bischak, L.Q. Flagg, K. Yan, et al., J. Am. Chem. Soc. 142 (2020) 7434–7442.
[30] L. Zhang, C. Liu, X. Wang, et al., Adv. Funct. Mater. 29 (2019) 1904856.
[31] L. Zhang, C. Liu, J. Zhang, et al., Adv. Mater. 30 (2018) 1804028.
[32] K. Yan, Z. Shen, B. Niu, et al., Sci. China Chem. 66 (2023) 1795–1803.
[33] K. Yao, S. Leng, Z. Liu, et al., Joule 3 (2019) 417–431.
[34] J. Peng, D. Walter, Y. Ren, et al., Science 371 (2021) 390–395.
[35] Y. Lin, L. Shen, J. Dai, et al., Adv. Mater. 29 (2017) 1604545.
[36] K. Yan, J. Chen, H. Ju, et al., J. Mater. Chem. A 6 (2018) 15495–15503.
[37] T. Niu, J. Lu, R. Munir, et al., Adv. Mater. 30 (2018) 1706576.
[38] S. Tan, I. Yavuz, M.H. Weber, et al., Joule 4 (2020) 2426–2442.
[39] D. Ma, X. He, J. He, et al., Chin. Chem. Lett. 34 (2023) 108629.